EVALUATION OF Fe-BASED OXYGEN CARRIERS SUPPORTED WITH Al_2O_3, ZrO_2 AND CeO_2 IN CHEMICAL LOOPING HYDROGEN GENERATION

Shiwei Ma, Wenguo Xiang*, Shiyi Chen

Key Laboratory of Energy Thermal Conversion and Control of Ministry of Education,

Southeast University, 210096Nanjing, China

*Email: *wgxiang@seu.edu.cn*

Abstract –Chemical looping hydrogen generation (CLHG) is a promising technology that can produce high-purity hydrogen with inherent CO_2 capture. It is composed of three steps, reduction by fuel gas, steam-iron process and air oxidation. Fe_2O_3 is currently the best candidate for CLHG with high CO_2 and H_2O selectivity and H_2 mole fraction in iron-steam reaction, and it is also of low cost and abundance in nature. However, pure Fe_2O_3 cannot meet the requirement of oxygen carriers in multi-cycles. It should be combined with support to improve its reactivity and stability, and eliminate potential sintering and carbon deposition. In this paper, Fe-based oxygen carriers, which consisted of 60wt% iron oxide and 40wt% support, were prepared by co-precipitation method with three supports including inert and reducible ones, i.e. Al_2O_3, ZrO_2 and CeO_2. Experiments were conducted in a batch fluidized bed with CO as fuel during multiple redox cycles for CLHG. The H_2 yield, carbon deposition, reactivity and redox stability of the oxygen carriers were analyzed to investigate the effects of supports as well as the fundamental mechanism. The experiments results showed that the properties of the oxygen carriers highly relied on the support and its interaction with iron oxide. The oxygen carrier supported by Al_2O_3 exhibited poor reactivity and stability, and the oxygen carrier supported by ZrO_2 led much carbon deposition, decreasing H_2 purity. However, the reducible support CeO_2, rendering fast oxygen transfer rate and the formation of perovskite-type $CeFeO_3$, demonstrated reactivity enhancement for Fe_2O_3, counteracted the negative effect originating from sintering and guaranteed the reactivity and stability of Fe_2O_3/CeO_2. In addition, the oxygen carrier supported by CeO_2 suppressed carbon deposition and H_2 with high purity could be attained. Overall, CeO_2 is a potential support for H_2 production with consideration of H_2 yield and purity.

INTRODUCTION

Hydrogen is an ideal energy carrier with a net calorific value of 121.00MJ/kg, higher than any other known fuel, and no pollutants or greenhouse gases are emitted into the atmosphere during the process of hydrogen utilization, as can be found in Chaubey et al. (2013). So hydrogen is an optimal solution for the energy supply in future. Also, Holladay et al. (2009) wrote that hydrogen was an important industrial material which can be widely used in the production of ammonia, gasoline, methanol, ethanol, etc. However, there is no hydrogen existing on the earth, owing to its highly active property, and it must be generated from other energy sources. It can be found in (Adanez et al., 2012) that steam methane reformation (SMR) is commercially proven, and it is currently the predominant technology for hydrogen production. Nevertheless, the process for SMR is complex and expensive, especially when CO_2 capture process is implemented.

Chemical looping hydrogen generation (CLHG) is a promising hydrogen production technology developed from chemical looping combustion (CLC). It can not only produce high purity hydrogen but also separate CO_2 inherently. CLHG consists of three reactors: fuel reactor (FR), steam reactor (SR) and air reactor (AR). The oxygen carrier, mostly iron oxide, circulates among the three reactors, converting hydrocarbons into hydrogen. For CO as fuel, the reactions in these three reactors can be described as follow.

In the FR, Fe_2O_3 is reduced to Fe or FeO, as shown in Eq. (1) to Eq. (3).

$$3Fe_2O_3 + CO \rightarrow 2Fe_3O_4 + CO_2 \quad (1)$$

$$Fe_3O_4 + CO \rightarrow 3FeO + CO_2 \quad (2)$$

$$Fe_3O_4 + 4CO \rightarrow 3Fe + 4CO_2 \quad (3)$$

In the SR, Fe and FeO are oxidized into Fe_3O_4, releasing H_2, as listed in Eq. (4) and Eq. (5).

$$3FeO + H_2O \rightarrow Fe_3O_4 + H_2 \quad (4)$$

$$3Fe + 4H_2O \rightarrow Fe_3O_4 + 4H_2 \quad (5)$$

In the AR, Fe_3O_4 is further oxidized and so Fe_2O_3 is regenerated, as can be seen in Eq. (6).

$$4Fe_3O_4 + O_2 \rightarrow 6Fe_2O_3 \quad (6)$$

Luo et al. (2015) wrote that the oxygen carrier material was the key issue related to the performance of chemical looping process. It would be an effective way to develop new oxygen carriers that can not only convert more fuel into hydrogen, but also decrease the carbon deposition and obtain H_2 of high purity. Kang et al. (2010a) wrote that although Fe_2O_3, CeO_2 and WO_3 could be all applied to CLHG, Fe_2O_3 was the most suitable oxygen carrier regarding to the CO_2 and H_2O selectivity and H_2 concentration at the outlet of SR. Moreover, Fe_2O_3 is attractive owing to its abundance, low cost and low toxicity.

In addition to the active metal oxides, supports are also indispensable part to the oxygen carriers for high reactivity and resistance to sintering, carbon deposition and attrition. There are many investigations on the comparison of different supports, such as Al_2O_3, $MgAl_2O_4$, TiO_2, SiO_2, ZrO_2, YSZ (yttrium-stabilized zirconia), for related CLC and CLR (Chemical Looping Reforming) regarding to the Fe-based oxygen carriers, which can be found in (Galinsky et al., 2015; Adánez et al., 2004; Chen et al., 2014). But the results cannot be directly applied in CLHG. The difference of CLHG from CLC/CLR is the reduction. Fe_2O_3 must be reduced to Fe/FeO in CLHG rather than merely Fe_3O_4 in CLC. However, Lin et al. (2016) wrote that Fe and FeO could facilitate carbon deposition, but this can be avoided in CLC because Fe_2O_3 is only reduced to Fe_3O_4. In addition, Tang et al. (2015) wrote that FeO could react with some supports, so the selection of supports is important for Fe-based oxygen carriers in CLHG. Many researches focused on the effects of the different inert supports for CLC and CLR, but the inert effects for CLHG are limited. Chen et al. (2011) wrote that H_2 yield of Fe-based oxygen carrier supported by Al_2O_3 was superior to that of TiO_2 due to the formation of unreactive $FeTiO_3$. It can be found in (Kosaka et al., 2015) that oxide ion conductors YSZ and GDC (gadolinia-doped ceria) could accelerate the reduction of Fe_2O_3 for H_2 storage, while CeO_2 and GDC would distinctly boost the reduction kinetics from FeO to Fe; furthermore, all these three supports could improve the steam-iron reaction rates compared to ZrO_2.

CeO_2 is a reducible support that is widely used in redox catalysis, such as automotive exhaust abatement, water gas shift and catalytic methane oxidation. It can be found in (Shi et al., 2008) that the promotion role of CeO_2 for the active metal in catalyst is due to its property of storing and releasing oxygen, which could accelerate the reduction of active metal. CeO_2 has been used in CLC as a reducible support. Bhavsar and Veser (2013a, 2013b) wrote that CeO_2, as a support for Ni-based and Fe-based oxygen carriers in CLC, could accelerate the reaction kinetics and enlarged the time window for total oxidation of methane compared to inert supports Al_2O_3 and SiO_2; more striking was that CeO_2 allowed for complete carrier conversion with H_2 or CH_4 as fuel. Liu et al. (2014) wrote that the oxygen carrier Fe_2O_3/Al_2O_3 with CeO_2 additive provided better average reaction rates in CLC with CO as fuel, for the vacancies inspired by CeO_2 could transfer oxygen quickly to the surface of the oxygen carrier by vacancy diffusion or even through oxygen tunnels formed by vacancies. Similarly, the improved performance for methane total oxidation with CeO_2 additive to Fe_2O_3 can be found in (Miller and Siriwardane, 2013). Furthermore, Bhavsar et al. (2016) wrote that oxygen carriers supported by gadolinia doped-ceria or lanthana-doped ceria showed even higher reactivity and oxygen capacity for CLC. For CLR, Li et al. (2010) wrote that the oxygen carrier Fe_2O_3/CeO_2 maintained high catalytic activity and selectivity during the conversion of methane to synthesis gas due to the oxygen mobility enhancement by the solid solution originated from Fe_2O_3 and CeO_2. Moreover, there are some researches on the chemical-looping steam methane reforming (CL-SMR) over the Fe_2O_3/CeO_2 oxygen carrier. It can be found in (Zhu et al., 2013) that Fe_2O_3/CeO_2 was a promising oxygen carrier in CL-SMR for its high redox activity and desired product yield of syngas and hydrogen. Zhu et al. (2014a) also wrote that CeO_2 modified Fe_2O_3 was a suitable material for the chemical hydrogen storage and production and Ce addition could decrease both the hydrogen reduction temperature and the temperature for water splitting reaction. In addition, Ce could be used to eliminate carbon deposition due to its redox properties and oxygen buffering capacity. Zheng et al. (2017) wrote that CeO_2 could reduce the carbon deposition for the reforming of methane. Sun et al. (2015) wrote that the oxygen carrier Fe_2O_3/Al_2O_3 modified by CeO_2 could effectively inhibit carbon deposition or Fe_3C formation in CLHG. Based on those findings, CeO_2 may be a promising support for Fe-based oxygen carriers with excellent performance in CLHG.

The present work investigated the effects of supports on H_2 yield, carbon deposition, reactivity and redox stability of Fe-based oxygen carriers for CLHG in batch fluidized bed. Al_2O_3 and ZrO_2, which are frequently encountered and perform well in chemical looping process, are included for comparison apart from CeO_2.

EXPERIMENTAL SECTION

OXYGEN CARRIER SYNTHESIS

The Fe-based oxygen carriers were prepared by co-precipitation, and the ratio of Fe_2O_3 and the inert support was kept 6:4. The calculated precursor nitrates for Fe_2O_3, $Fe(NO_3)_3{\cdot}9H_2O$ (AR, Nanjing Chemical Reagent Co., Ltd), and metal oxide supports, $Ce(NO_3)_3{\cdot}6H_2O$ (99.5%, Aladdin), $Al(NO_3)_3{\cdot}9H_2O$ (AR, Greagent), or $Zr(NO_3)_4{\cdot}5H_2O$ (AR, Greagent), were put into solution with deionized water. The solution was sufficiently blended and heated in a magnetic stirrer until the temperature reached 70℃. Then a 25%~28% ammonia solution was gradually introduced into the mixture to increase the PH of the solution to 9. It was then aged for 12 h under room temperature. Afterwards, the resulting precipitate was filtered and dried at 110℃ in a drier for 24 h. The resulting solids are subsequently subjected to decomposition at 350℃ for 2 h and sintered at 900℃ for 2 h in a muffle oven. Then the particles were crushed and sieved to get powder in the size range of 0.150~0.250 mm for experiments.

OXYGEN CARRIER CHARACTERIZATION

X-ray powder diffraction (XRD) was implemented to study the crystal phase compositions. XRD patterns were recorded using a Rigaku SmartLab X-ray diffractometer with Cu-Kα radiation operating at 3 kW. The sample scans were performed in a step-scan mode between an angle range of 20~90° (2θ), with a step size rate of 0.1°/s. Scanning electron microscopy (SEM) and Energy Dispersive Spectrometer(EDS) was performed on an Ultra Plus (Carl Zeiss AG) microscope to study the morphology of oxygen carriers.

EXPERIMENTAL REACTOR AND PROCEDURE

A laboratory-scale batch fluidized bed reactor was used in the test as shown in Fig.1. This system was comprised of three parts, a gas distribution system, a fluidized bed reactor, and an off-gas treatment system. In the gas distribution system, distilled water was pumped into a steam generator and heated into steam, whereas CO, N_2 and O_2 were sent into the reactor through the mass flow controllers. The reactor was a quartz fluidized bed, which had a length of 750 mm and an inner diameter of 22 mm with a porous quartz plate placed 150 mm from the bottom. The quartz tube was heated by an electric furnace with a temperature controller. In the off-gas treatment system, the outlet flue gas was first condensed to remove water, and then dried by silica gel. The off-gas was finally sent into the gas analyzer.

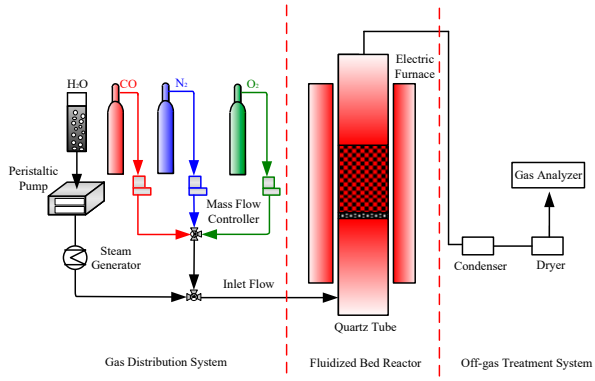

Fig. 1. Schematic diagram of the experimental setup

In each test, the oxygen carrier was 10 g, which was placed on the porous quartz plate, and the furnace was heated to the desired temperature under nitrogen atmosphere, then the particles were exposed to reducing and oxidizing atmosphere. There were three stages in a cycle, including CO reduction stage (35 min), steam oxidation stage (20 min) and air oxidation stage (15 min). The experiments were carried out at isothermal condition with a constant total flow rate of 0.5 L/min, while, in steam oxidation stage, nitrogen flow rates was 0.35 L/min and the H_2O (l) injected into the furnace was 0.20 mL/min. The minimum fluidized velocity, u_{mf}, of the particles was 0.018 m/s at 850 °C, and the gas velocity u_g was 0.101 m/s, i.e., 5.6 u_{mf}, sufficient to fluidize the oxygen carrier. Gas flow rates were adjusted so that there was 30% CO in reduction stage and 16% O_2 in air oxidation stage balanced with nitrogen. Nitrogen blowing stage was conducted after every stage. In order to investigate the carbon deposition of the oxygen carriers and to avoid CO contamination from the reduction period, the nitrogen blowing stage between reduction stage and steam oxidization stage lasted for 40~50 min until the concentration of CO and CO_2 went down to zero.

DATE EVALUATION

The total volume flow rate of the off-gas F_{out} is defined as:

$$F_{out} = \frac{F_{N_2,in}}{1 - X_{CO} - X_{CO_2} - X_{H_2}} \tag{7}$$

Where $F_{N_2,in}$ is the volume flow rate of the inlet nitrogen, X_{CO}, X_{CO_2} and X_{H_2} are the measured concentrations of CO, CO_2 and H_2 respectively.

The volume flow rate of CO_2 in the off-gas is:

$$F_{CO_2} = F_{out} X_{CO_2} \tag{8}$$

The volume flow rate of H_2 in the off-gas for the steam oxidization period is:

$$F_{H_2} = F_{out} X_{H_2} \tag{9}$$

The H_2 yield in the steam oxidizing period is:

$$V_{H_2} = \int_0^t F_{H_2} \tag{10}$$

The gas yield of carbonaceous gases, including CO and CO_2, in the steam oxidization period is:

$$V_{CO_x} = \int_0^t F_{out} \left(X_{CO_2} + X_{CO} \right) \tag{11}$$

The H_2 purity in the steam oxidization period is:

$$\alpha_{H_2} = 1 - \frac{V_{CO_x}}{F_{out}} \tag{12}$$

RESULTS AND DISCUSSION

EFFECT OF SUPPORTS ON H_2 YIELD

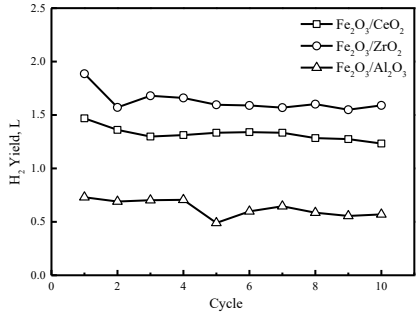

Fig. 2. Effect of cycle number on H_2 yield for oxygen carriers with different supports at 850°C

Fig. 2 shows the H_2 yields in 10 redox cycles for oxygen carriers with different supports at 850°C. After three cycles, the H_2 yields for all the investigated oxygen carriers came to a relatively stable state, decreasing slightly with cycle number, which indicated that the structure of the oxygen carriers tended to stabilize. The H_2 yields followed the sequence: Fe_2O_3/ZrO_2 > Fe_2O_3/CeO_2 > Fe_2O_3/Al_2O_3. And the average H_2 yields from the 3rd to 10th cycle were 1.60 L, 1.30 L, 0.61 L, respectively. Fe_2O_3/ZrO_2 showed high H_2 yield due to the high phase stability and thermal stability of ZrO_2. For Fe_2O_3/CeO_2, it can be found in (Galinsky et al., 2015) that the poor performance of Fe_2O_3/CeO_2 resulted from solid-state migration of iron cations and subsequent enrichment on the oxygen carrier surface, which led to sintering and lowered lattice oxygen accessibility. As a note of caution, however, Bhavsar and Veser (2013b) wrote that although CeO_2 demonstrated reducibility compared to no reducibility for ZrO_2 and Al_2O_3, the oxygen carrying capacity was negligible compared to typical metals, such as Fe_2O_3 and NiO. The terrible H_2 yield for Fe_2O_3/Al_2O_3 could be attributed to the generation of inactive spinel $FeAl_2O_4$, which can be found in (Svoboda et al., 2007), or sintering problem that can be found in (Nandy et al., 2016). Although the oxygen carrier Fe_2O_3/ZrO_2 is the best one in view of H_2 yield, carbon deposition is another important factor which have a serious impact on the H_2 purity and should be sufficiently considered, especially when the hydrogen is intended to applied in the fuel cell.

CARBON DEPOSITION

The hydrogen produced in CLHG with CO as fuel and Fe_2O_3 as oxygen carrier can reach high purity above 99%, the reason why the purity cannot achieve 100% is the carbon deposition generated in the FR, as can be found in (Cho et al., 2014). The related reaction is called as Boudouard reaction, see below in Eq. (13).

$$2CO \rightarrow CO_2 + C \tag{13}$$

The carbon deposition generated will then react with H_2O, leading to the production of CO and CO_2, leading to the contamination of H_2, as shown in Eq. (8) and (9).

$$C + H_2O \rightarrow CO + H_2 \tag{14}$$

$$CO + H_2O \rightarrow CO_2 + H_2 \tag{15}$$

Many factors can influence the carbon deposition, such as reaction pressure, temperature, composition and concentration of fuel gas, and the quality of the available lattice oxygen from oxygen carrier, which can be found in (Wang et al., 2008).

Carbon deposition could be converted to CO or CO_2 both in steam oxidation stage and air oxidation stage, however, the attention was paid to the steam oxidation stage in this paper, which exerted direct influence on the H_2 purity. CO and CO_2 could not detected by the gas analyzer under the experimental condition described above, viz. the concentrations of CO and CO_2 in the steam oxidation stage were beyond the detection limits (50ppmv) of the gas analyzer. Therefore, 100% CO (flow rate 0.5L/min) was sent into the fluidized bed instead of 30% to investigate the resistance of the oxygen carriers to carbon deposition. The H_2 purities corresponding to the three oxygen carriers are illustrated below in Fig.3.

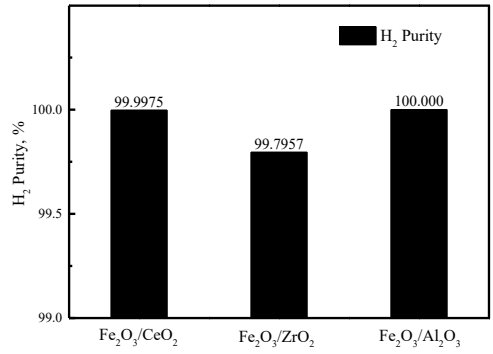

Fig. 3. Effect of different supports on H_2 purity at 850°C

It can been seen in Fig.3 that the H_2 purities followed the sequence: $Fe_2O_3/Al_2O_3 > Fe_2O_3/CeO_2 > Fe_2O_3/ZrO_2$. Interestingly, this sequence is quite the opposite to that of H_2 yields. It can also be found in (Kang et al., 2010b) that ZrO_2 supported oxygen carrier showed more carbon deposition than that of CeO_2. The reason for low carbon deposition on Fe_2O_3/CeO_2 is that CeO_2 can provide oxygen species from lattice oxygen to oxidize the surface carbon, producing CO or CO_2. However, for Fe_2O_3/ZrO_2, plenty of Fe or FeO originating from deep reduction promote the Boudouard reaction, leading to much carbon deposition. The gas analyzer could not detect CO or CO_2 generated from the carbon deposition for Fe_2O_3/Al_2O_3 probably due to the sintering of the particle surface and the resulting reduction of active sites Fe or FeO. In addition, the element distribution of the oxygen carriers obtained after the 11th reduction stage (30% CO) was characterized by EDS. The result showed that the weight ratios of carbon element on the surface of the reduced oxygen carriers were 2.46%, 4.56% and 11.45% for Fe_2O_3/Al_2O_3, Fe_2O_3/CeO_2 and Fe_2O_3/ZrO_2 respectively, which was consistent with the result indicated by Fig.3.

It can be found in (Hotza and Diniz Da Costa, 2008) that the fuel cell with a polymeric electrolyte membrane (PEM) had been chosen by most of the automotive companies as the power source for future vehicles, however, Bohn et al. (2008) wrote that the level of CO contamination for the hydrogen used in a PEM fuel cell must be kept below ~50 ppm, so as not to poison the platinum clusters on the anode. Therefore, only the hydrogen yielded by Fe_2O_3/Al_2O_3 and Fe_2O_3/CeO_2 can meet the requirement. However, the H_2 yield for Fe_2O_3/Al_2O_3 was lower and the reduction rate from the 3rd to 10th cycle was 19.0%, versus 5.0% for that of Fe_2O_3/CeO_2. To sum up, Fe_2O_3/CeO_2 was the most suitable oxygen carrier for H_2 production with consideration of H_2 yield and purity in CLHG.

REACTIVITY AND REDOX STABILITY

The reactivity and stability of Fe_2O_3/CeO_2 was investigated, since Fe_2O_3/CeO_2 showed the best performance, by comparing the CO_2 concentration for the reduction stage in redox cycles. As can be seen in Fig.4, the peak values of CO_2 concentration decreased from 16.6% to 14.9% from the 1st to 3rd cycle, but those for the 3rd and 10th cycles were very close to each other, and the CO_2 concentration curves were almost the same, which indicated the satisfactory stability of reactivity for Fe_2O_3/CeO_2. It can also be found in Fig.4 that the CO_2 concentration at the end of the reduction stage in the 3rd and 10th cycles was higher than that in the 1st cycle, with the highest one in the 10th cycle. This phenomenon can be attributed to the perovskite-type $CeFeO_3$ formed in the redox cycles, which could intensify the oxygen mobility, promoting the reactivity of Fe_2O_3/CeO_2, counteract the negative impact originating from sintering and guarantee the stability of Fe_2O_3/CeO_2, as can be found in (Zhu et al., 2014b).

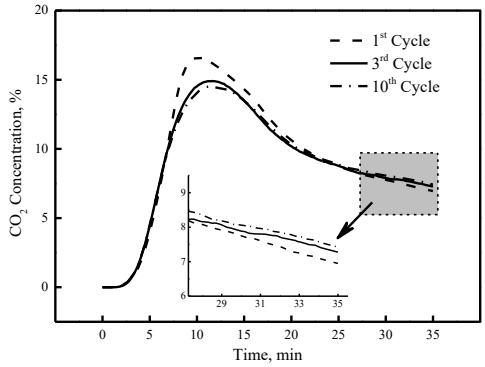

Fig. 4. CO_2 concentration in reduction stage for Fe_2O_3/CeO_2 in the 1st, 3rd and 10th cycles at 850°C

MORPHOLOGY AND COMPONENTS

The oxygen carrier Fe_2O_3/CeO_2 was further investigated in view of morphology and components by SEM and XRD. The SEM and XRD analysis of Fe_2O_3/CeO_2 are shown in Fig. 5 and Fig. 6, respectively. As can be seen in Fig.5, grains with a size of 0.2~0.5μm over the surface of the particles led to the porous structure for fresh oxygen carrier, however, smaller grains agglomerated together and sintering occurred after redox cycles, blocking the pores and preventing sufficient contact between reactant gas and oxygen carrier. Nevertheless, the oxygen carrier still kept high reactivity and H_2 yield along with the redox cycles due to the reducible support, CeO_2, as shown in Fig.2 and Fig.4.

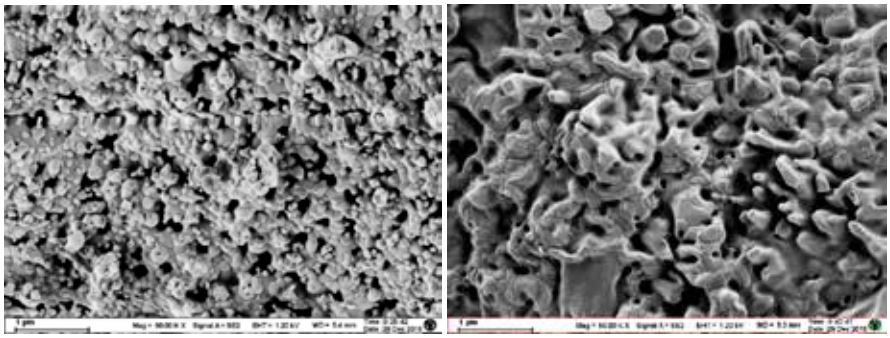

(a) Fresh (b) After 10 redox cycles

Fig.5. SEM images of the oxygen carrier Fe_2O_3/CeO_2

Fig.6 shows XRD patterns of Fe_2O_3/CeO_2. In its fresh state, only Fe_2O_3 and CeO_2 existed. After air oxidation in the 10th cycle, the intensity of CeO_2 decreased seriously, indicating the iron enrichment on the oxygen carrier surface, which promoted sintering. The XRD pattern of Fe_2O_3/CeO_2 for the reduction state verified not only the existence of Fe and FeO, but also $CeFeO_3$, which could intensify the oxygen mobility and promote the reactivity of Fe_2O_3/CeO_2, just as the illustration in Fig.4.

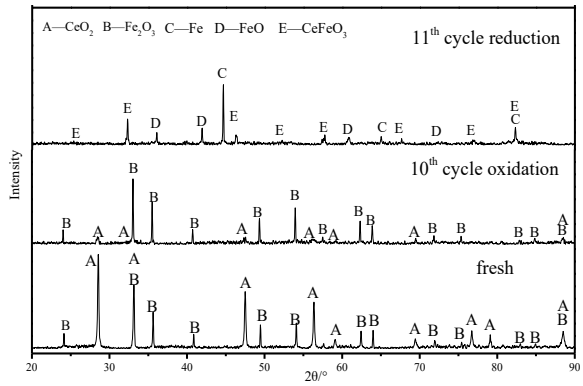

Fig.6. XRD patterns of the oxygen carrier Fe_2O_3/CeO_2

CONCLIUSIONS

Three Fe-based oxygen carriers, supported by Al_2O_3, ZrO_2 and CeO_2, were prepared by co-precipitation and investigated in a batch fluidized bed at 850°C using CO as fuel for CLHG. The conclusions were drawn as below. (1) The properties of the oxygen carriers, e.g. reactivity and stability, mainly depended on the support and its interaction with iron oxides; (2) The reactivity and H_2 yield for the oxygen carriers followed the sequence: Fe_2O_3/ZrO_2 > Fe_2O_3/CeO_2 > Fe_2O_3/Al_2O_3, however, the resistance to carbon deposition followed the reverse sequence: Fe_2O_3/Al_2O_3> Fe_2O_3/CeO_2 > Fe_2O_3/ZrO_2; Fe_2O_3/CeO_2 was the most suitable one for CLHG with the consideration of H_2 yield and carbon deposition in CLHG; (3) Fe_2O_3/CeO_2 suffered sintering in redox cycles, but it still kept high reactivity, redox stability and H_2 yield; (4) XRD analysis verified the iron enrichment on the oxygen carrier surface, which promoted sintering, and the formation of perovskite-type $CeFeO_3$ that could guarantee the reactivity and stability of Fe_2O_3/CeO_2.

ACKNOWLEDGEMENTS

The authors gratefully express thanks to the National Natural Science Foundation of China (51576042), National Program on Basic Research Project (2016YFB0600802), and Natural Science Foundation of Jiangsu (BK20160672) for financial support of this research.

NOTATION

F	gas flow rate, L/min	X	gas volume concentration, %
V	volume, L	u_g	gas velocity, m/s
u_{mf}	minimum fluidized velocity, m/s	α_{H_2}	H_2 purity, %

REFERENCES

Adánez, J., de Diego, L. F., García-Labiano, F., Gayán, P., Abad, A., Palacios, J. M. 2004. Selection of oxygen carriers for chemical-looping combustion. Energy & Fuels 18, (2), 371-377.

Adanez, J., Abad, A., Garcia-Labiano, F., Gayan, P., de Diego, L.F. 2012. Progress in chemical-looping combustion and reforming technologies. Progress in Energy and Combustion Science 38, (2), 215-282.

Bhavsar, S., Isenberg, N., More, A., Veser, G. 2016. Lanthana-doped ceria as active support for oxygen carriers in chemical looping combustion. Applied Energy 168, 236-247.

Bhavsar, S., Veser, G. 2013a. Bimetallic Fe-Ni oxygen carriers for Chemical Looping Combustion. Industrial & Engineering Chemistry Research 52, (44), 15342-15352.

Bhavsar, S., Veser, G. 2013b. Reducible supports for Ni-based oxygen carriers in chemical looping combustion. Energy & Fuels 27, (4), 2073-2084.

Bohn, C. D., Mulle, C. R., Cleeton, J. P., Hayhurst, A. N., Davidson, J. F., Scott, S. A., Dennis, J. S. 2008. Production of very pure hydrogen with simultaneous capture of carbon dioxide using the redox reactions of iron oxides in packed beds. Industrial & Engineering Chemistry Research 47, (20), 7623-7630.

Chaubey, R., Sahu, S., James, O. O., Maity, S. 2013. A review on development of industrial processes and emerging techniques for production of hydrogen from renewable and sustainable sources. Renewable and Sustainable Energy Reviews 23, 443-462.

Chen, S., Shi, Q., Xue, Z., Sun, X., Xiang, W. 2011. Experimental investigation of chemical-looping hydrogen generation using Al_2O_3 or TiO_2-supported iron oxides in a batch fluidized bed. International Journal of Hydrogen Energy 36, (15), 8915-8926.
Chen, Y., Galinsky, N., Wang, Z., Li, F. 2014. Investigation of perovskite supported composite oxides for chemical looping conversion of syngas. Fuel 134, 521-530.
Cho, W. C., Lee, D. Y., Seo, M. W., Kim, S. D., Kang, K.S., Bae, K. K., Jeong, S. U., Park, C. S. 2014. Continuous operation characteristics of chemical looping hydrogen production system. Applied Energy 113, 1667-1674.
Galinsky, N. L., Shafiefarhood, A., Chen, Y., Neal, L., Li, F. 2015. Effect of support on redox stability of iron oxide for chemical looping conversion of methane. Applied Catalysis B: Environmental 164, 371-379.
Holladay, J. D., Hu, J., King, D. L., Wang, Y. 2009. An overview of hydrogen production technologies. Catalysis Today 139, (4), 244-260.
Hotza, D., Diniz Da Costa, J. C. 2008. Fuel cells development and hydrogen production from renewable resources in Brazil. International Journal of Hydrogen Energy 33, (19), 4915-4935.
Kang, K. S., Kim, C. H., Bae, K. K., Cho, W. C., Kim, S. H., Park. C. S. 2010a. Oxygen-carrier selection and thermal analysis of the chemical-looping process for hydrogen production. International Journal of Hydrogen Energy 35, (22), 12246-12254.
Kang, K. S., Kim, C. H., Cho, W. C., Bae, K. K., Woo, S. W., Park, C. S. 2010b. Redox cycling of $CuFe_2O_4$ supported on ZrO_2 and CeO_2 for two-step methane reforming/water splitting. International Journal of Hydrogen Energy 35, (2), 568-576.
Kosaka, F., Hatano, H., Oshima, Y., Otomo, J. 2015. Iron oxide redox reaction with oxide ion conducting supports for hydrogen production and storage systems. Chemical Engineering Science 123, 380-387.
Kothari, R., Buddhi, D., Sawhney, R. L. 2008. Comparison of environmental and economic aspects of various hydrogen production methods. Renewable and Sustainable Energy Reviews 12, (2), 553-563.
Li, K., Wang, H., Wei, Y., Yan, D. 2010. Direct conversion of methane to synthesis gas using lattice oxygen of CeO_2-Fe_2O_3 complex oxides. Chemical Engineering Journal 156, (3), 512-518.
Lin, C., Qin, W., Dong, C. 2016. Reduction effect of α-Fe_2O_3 on carbon deposition and CO oxidation during chemical-looping combustion. Chemical Engineering Journal 301, 257-265.
Liu, F., Chen, L., Neathery, J. K., Saito, K., Liu, K. 2014. Cerium oxide promoted iron-based oxygen carrier for chemical looping combustion. Industrial & Engineering Chemistry Research 53, (42), 16341-16348.
Luo, S., Zeng, L., Fan, L. S. 2015. Chemical looping technology: oxygen carrier characteristics. Annual review of chemical Biomolecular Engineering 6, 53-75.
Miller, D. D., Siriwardane, R. 2013. Mechanism of methane chemical looping combustion with hematite promoted with CeO_2. Energy & Fuels 27, (8), 4087-4096.
Nandy, A., Loha, C. M., Gu, S., Sarkar, P., Karmakar, M. K., Chatterjee, P. K. 2016. Present status and overview of chemical looping combustion technology. Renewable and Sustainable Energy Reviews 59, 597-619.
Shi, F., Tse, M. K., Pohl, M. M., Radnik, J., Bruckner, A., Zhang, S. M., Beller, M. 2008. Nano-iron oxide-catalyzed selective oxidations of alcohols and olefins with hydrogen peroxide. Journal of Molecular Catalysis A: Chemical 292, (1-2), 28-35.
Sun, S., Zhao, M., Cao, L., Zhang S., Zeng D., Xiao, R. 2015. Performance of CeO_2-modified iron-based oxygen carrier in the chemical looping hydrogen generation process. Energy & Fuels 29, (11), 7612-7621.
Svoboda, K., Slowinski, G., Rogut, J., Baxter, D. 2007. Thermodynamic possibilities and constraints for pure hydrogen production by iron based chemical looping process at lower temperatures. Energy Conversion and Management 48, (12), 3063-3073.
Tang, M., Xu, L., Fan, M. 2015. Progress in oxygen carrier development of methane-based chemical-looping reforming: A review. Applied Energy 151, 143-156.
Wang, B., Yan, R., Lee, D. H., Liang, D. T., Zheng, Y., Zhao, H., Zheng, C. 2008. Thermodynamic Investigation of carbon deposition and sulfur evolution in chemical looping combustion with syngas. Energy & Fuels 22, (2), 1012-1020.
Zheng, Y., Li, K., Wang, H., Tian, D., Wang, Y., Zhu, X., Wei, Y., Zheng, M., Luo, M. 2017. Designed oxygen carriers from macroporous $LaFeO_3$ supported CeO_2 for chemical-looping reforming of methane. Applied Catalysis B: Environmental 202, 51-63.
Zhu, X., Sun, L., Zheng, Y., Wang, H., Wei, Y., Li, K. 2014a. CeO_2 modified Fe_2O_3 for the chemical hydrogen storage and production via cyclic water splitting. International Journal of Hydrogen Energy 39, (25), 13381-13388.
Zhu, X., Li, K., Wei, Y., Wang, H., Sun, L. 2014b. Chemical-looping steam methane reforming over a CeO_2–Fe_2O_3 oxygen carrier: evolution of its structure and reducibility. Energy & Fuels 28, (2), 754-760.
Zhu, X., Wei, Y., Wang, H., Li, K. 2013. Ce–Fe oxygen carriers for chemical-looping steam methane reforming. International Journal of Hydrogen Energy 38, (11), 4492-4501.